On the energy spectrum of rapidly rotating forced turbulence

Manohar K. Sharma, Mahendra K. Verma, and Sagar Chakraborty

Citation: Physics of Fluids **30**, 115102 (2018); doi: 10.1063/1.5051444
View online: https://doi.org/10.1063/1.5051444
View Table of Contents: http://aip.scitation.org/toc/phf/30/11
Published by the American Institute of Physics

On the energy spectrum of rapidly rotating forced turbulence

Manohar K. Sharma,[a)] Mahendra K. Verma,[b)] and Sagar Chakraborty[c)]
Department of Physics, Indian Institute of Technology Kanpur, Uttar Pradesh 208016, India

(Received 8 August 2018; accepted 2 October 2018; published online 16 November 2018)

In this paper, we investigate the statistical features of a fully developed, forced, rapidly rotating, turbulent system using numerical simulations and model the energy spectrum that fits well with the numerical data. Among the wavenumbers (k) larger than the Kolmogorov dissipation wavenumber, the energy is distributed such that the suitably non-dimensionalized energy spectrum is $\bar{E}(\bar{k}) \approx \exp(-0.05\bar{k})$, where the overbar denotes appropriate non-dimensionalization. For the wavenumbers smaller than that of forcing, the energy in a horizontal plane is much more than that along the vertical rotation-axis. For such wavenumbers, we find that the anisotropic energy spectrum, $E(k_\perp, k_\parallel)$, follows the power law scaling, $k_\perp^{-5/2}k_\parallel^{-1/2}$, where "$\perp$" and "$\parallel$," respectively, refer to the directions perpendicular and parallel to the rotation axis; this result is in line with the Kuznetsov–Zakharov–Kolmogorov spectrum predicted by the weak inertial-wave turbulence theory for the rotating fluids. *Published by AIP Publishing.* https://doi.org/10.1063/1.5051444

I. INTRODUCTION

Rotating turbulence[1]—turbulence in rotating fluids—is a commonly occurring phenomenon in geophysical and astrophysical flows. It also occurs in engineering flows like the ones in turbo-machinery and reciprocating engines with swirl and tumble. The large-scale structures of the turbulent system are affected by rotation due to the Coriolis force that acts in the plane perpendicular to the direction of angular velocity. Intriguingly, the scaling law of the energy spectrum in the inertial range changes with the rotation rate in a way so as to two-dimensionalize the three-dimensional (3D) fluid turbulence. It is well known that Kolmogorov[2,3] proposed an inertial range energy spectrum for homogeneous and isotropic 3D hydrodynamics turbulence, $E(k) \sim \epsilon^{2/3}k^{-5/3}$, where ϵ is the constant energy dissipation rate. The Kolmogorov spectrum is quite universal and observed in a plethora of other realistic settings, e.g., shear flows,[4] viscoelastic fluids,[5] buoyancy-driven systems,[6,7] and jet flows.[8] On the other hand, the energy cascade for the two-dimensional (2D) turbulence system shows dual behavior:[9–13] an inverse cascade at large scales with $E(k) \sim k^{-5/3}$ and a forward cascade of enstrophy at relatively small scales with $E(k) \sim k^{-3}$.

The energy spectrum becomes more complex in the presence of rotation in the turbulent system, and there is no unanimity about the form of the inertial range energy spectrum among the researchers. The largest wavenumber up to which the Coriolis force dominates over the nonlinearity is specified by the Zeman wavenumber, $k_\Omega \equiv (\Omega^3/\epsilon)^{1/2}$; larger scales corresponding to $k \lesssim k_\Omega$ are affected the most by the rotational effects. Here, Ω is the magnitude of the angular velocity. Be it analytical, numerical, or experimental investigations of either the forced or the decaying rotating turbulent fluid, it is generally found[14–39] that the energy spectrum for the rotation dominated wavenumbers scales as k^{-m}, where $m \in [2, 3]$. Apart from these power-law scalings for relatively larger scales, the energy spectrum for the smaller scales in rotating turbulence is equally enigmatic. In addition to the characteristic energy spectrum, the inverse cascade of energy is a prominent feature of rotating turbulence which has been studied experimentally as well as numerically.[23,30,35,40–43] While one observes[22,44] a forward cascade of energy in the vertical planes (the planes containing the direction of rotation), as far as the horizontal planes are concerned, there is usually a forward cascade of energy at the small horizontal scales and an inverse energy cascade at the large horizontal scales. The inverse cascade yields coherent columnar structures in the flow. There is also evidence[35,45] of non-local energy transfers in rotating turbulence.

In nonrotating 3D turbulent fluids, subsequent to a model proposed by Kraichnan[46] for the kinetic energy spectrum in the far dissipation range, Pao[47] and Pope[48] separately proposed models which are applicable in both the inertial and the dissipation ranges. These two model spectra, respectively, are $E(k) = \mathrm{K_o}\epsilon^{2/3}k^{-5/3}\exp(-\frac{3}{2}\alpha\nu\epsilon^{-1/3}k^{4/3})$, where $\mathrm{K_o}$ is the Kolmogorov constant and ν is the kinematic viscosity, and $E(k) = C\epsilon^{2/3}k^{-5/3}f_L(kL)f_\eta(k\eta)$, where C is a real constant, L is the integral length scale, η is the Kolmogorov length scale, and f_L and f_η are the two non-dimensional functions.[48] Another widely used typical phenomenological form of the energy spectrum in the far dissipation range of 3D isotropic homogeneous turbulence is given by $E(k) \sim (k/k_\eta)^\gamma \exp[-\beta(k/k_\eta)^n]$, where γ, β, and n are the real constants and k_η is the Kolmogorov dissipation scale. The values of γ, β, and n are often debated in the turbulence community. While $n = 1$ (cf. Ref. 49 supporting $n = 2$) is agreed upon by many researchers,[50–54] there is relatively more disagreement about the value[46,55–57] of γ (=3, −1.6, −2, 3.3) and the value[55,57,58] of β (=4.9, 7.1, 5.2). Needless to say, as far as the more complex problem of the forced rotating turbulence is concerned, the issue of such an

[a)]Electronic mail: kmanohar@iitk.ac.in
[b)]Electronic mail: mkv@iitk.ac.in
[c)]Electronic mail: sagarc@iitk.ac.in

energy spectrum is even wider open. Given the uncertainty in the two exponents, the usage of this energy spectrum is debatable. In fact, to the best of our knowledge, no one has reported such an energy spectrum for smaller scales that extend far into the dissipation range of the forced rotating fluid turbulence.

Recently, Sharma *et al.*[59] investigated the statistical behavior of the rapidly rotating decaying turbulence. They reported that a major fraction of the total energy is confined in the Fourier modes (±1, 0, 0) and (0, ±1, 0), which correspond to the largest coherent columnar structure in the flow. These modes contain approximately 85 percent of the total energy of the system. Furthermore, they also proposed a model for the energy spectrum, $E(k) \sim C\epsilon_\omega^{2/3}k^{-3}\exp[-C(k/k_d)^2]$ in the region $k \geq 2k_\eta$. Here $k_d \equiv \epsilon^{1/6}/\sqrt{\nu}$, ϵ_ω is the enstrophy dissipation rate, C is a constant, and k_η is the Kolmogorov dissipation wavenumber. There is no reason to believe *a priori* that these results should hold good for the forced rotating turbulence system. In fact, the introduction of forcing at an intermediate scale—corresponding wavenumber being k_f—breaks the kinetic energy spectrum into two disjoint regions: larger scales $k < k_f$ and smaller scales $k > k_f$. Contrary to what has been observed in the decaying case, the energy spectrum in the forced case shows power law scaling close to $E(k_\perp, k_\parallel) \sim k_\perp^{-5/2}k_\parallel^{-1/2}$ in highly anisotropic large scales. (The subscripts "⊥" and "∥," respectively, refer to the directions perpendicular and parallel to the rotation axis.) In the rather isotropic far dissipation range, the energy spectrum becomes an exponential function of "$-k$." Additionally, although we have observed that (±1, 0, 0) and (0, ±1, 0) still contain a major fraction of the total energy, the energy content in the intermediate and the smaller scales is much more than that for the decaying rotating turbulent; as a result, one observes rather diffused columnar structures in the case of forced rotating turbulence. The main aim of our paper is to elaborate on these interesting results and to contrast the forced turbulence with the decaying one.

However, before we start presenting the results in a systematic manner, let us clearly describe our model system.

II. THE MODEL SYSTEM

The governing equation of a forced incompressible fluid flow in the rotating reference frame is

$$\frac{\partial \mathbf{u}}{\partial t} + (\mathbf{u}\cdot\nabla)\mathbf{u} = -\nabla p - 2\boldsymbol{\Omega}\times\mathbf{u} + \nu\nabla^2\mathbf{u} + \mathbf{f}, \tag{1}$$

$$\nabla\cdot\mathbf{u} = 0, \tag{2}$$

where $\mathbf{u}$ is the velocity field, $\boldsymbol{\Omega} = \Omega\hat{z}$ is the angular velocity of the rotating frame, p is the pressure field which includes contributions from centrifugal acceleration, ν is the kinematic viscosity, $-2\boldsymbol{\Omega}\times\mathbf{u}$ is the Coriolis acceleration, and $\mathbf{f}$ is the force field.

We have simulated these equations in a cube of size $(2\pi)^3$ with the periodic boundary condition on all the sides using the pseudo-spectral code, Tarang.[60,61] We have used the fourth-order Runge-Kutta method for time stepping and the Courant-Friedrichs-Lewy (CFL) condition to optimize the time stepping (Δt) and 2/3 rule for dealiasing. Our simulations are with grid-resolutions of 512^3 and 1024^3, and a constant rotation rate $\Omega = 32$ which corresponds to the Rossby number (Ro) of the order of 10^{-3}. One may recall that $\mathrm{Ro} \equiv U/\Omega L$, with U and L, respectively, being the large scale velocity and the corresponding length scale, is the ratio of the magnitudes of $(\mathbf{u}\cdot\nabla)\mathbf{u}$ and the Coriolis acceleration. We have used our forcing scheme in such a way that it supplies constant energy and no kinetic helicity in the flow. In the Fourier space, the forcing function ($\hat{\mathbf{f}}(\mathbf{k})$) is taken as

$$\hat{\mathbf{f}}(\mathbf{k}) = \frac{\epsilon_{in}\hat{\mathbf{u}}(\mathbf{k})}{n_f\left[\hat{\mathbf{u}}(\mathbf{k})\hat{\mathbf{u}}^*(\mathbf{k})\right]}, \tag{3}$$

where n_f is the total number of modes at which the forcing is active and ϵ_{in} is the energy input rate. The phase of $\hat{\mathbf{f}}(\mathbf{k})$ is chosen randomly at every time step. Other relevant parameters of our simulations are tabulated in Table I.

TABLE I. Parameters of the simulation: the grid-resolution N, the forcing wavenumber band k_f, the rotation rate Ω, the kinematic viscosity ν, the final eddy turn-over time t_f, the energy supply rate ϵ, the Rossby number Ro, the Reynolds number Re, the Zeman wavenumber k_Ω, $k_{\max}\eta$, and the Kolmogorov dissipation wavenumber k_η.

N	512^3	1024^3
k_f	40-41	80–82
Ω	32	32
ν	0.001	0.001
t_f	56	3
ϵ	0.40	0.80
Ro	0.007	0.005
Re	1736	1786
k_Ω	286	202
k_η	141	168
$k_{\max}\eta$	4.4	3.0

We have used the data corresponding to the time frame $t = 45$ of 512^3 grid resolution as an initial condition for 1024^3 grid resolution. The system evolve up to $t = 3$ eddy turn-over time for 1024^3 grid resolution. We find that $k_{\max}\eta > 1.5$ for the simulation, where η is Kolmogorov's length scale, which shows that our simulation is well resolved. We have also ensured that the data are collected from the steady state. Additionally, by working with the two grid-resolutions, the results presented in this paper have been shown to be grid independent.

III. QUASI-TWO-DIMENSIONALIZATION

The Coriolis force affects the perpendicular components of velocity field $\mathbf{u}_\perp = u_x\hat{\mathbf{x}} + u_y\hat{\mathbf{y}}$, and this force is the primary reason for the quasi-two-dimensionalization (2D) of three-dimensional (3D) turbulent flow. Below we present evidence for the quasi-two-dimensional nature of the flow.

A. Strong anisotropy

We know that, by definition, the Coriolis force is dominant at wavenumbers smaller than the Zeman wavenumber. In Fig. 1, we plot the anisotropy parameter $A \equiv E_\perp/2E_\parallel$ as a function of wavenumber. Here, $E_\perp \equiv E_x + E_y$ and $E_\parallel \equiv E_z$ [with $E_x \equiv \int(u_x^2/2)d\mathbf{r}$, $E_y \equiv \int(u_y^2/2)d\mathbf{r}$, and $E_z \equiv \int(u_z^2/2)d\mathbf{r}$]. It is obvious from the figure that there is strong anisotropy ($A \gg 1$), and hence quasi-two-dimensionalization, at larger

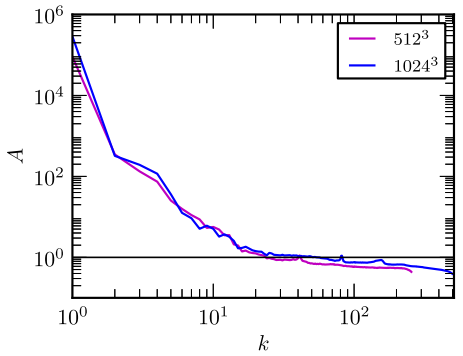

FIG. 1. Anisotropy of the forced rotating turbulent system vs. wavenumber at $t = t_f$ for grid simulation of 512^3 grid resolution (magenta) and 1024^3 grid resolution (blue).

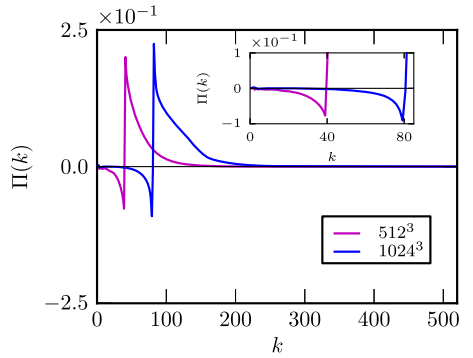

FIG. 2. Plot of kinetic energy flux $\Pi(k)$ vs. k of the 3D velocity field at $t = t_f$ for 512^3 grid resolution (magenta) and 1024^3 grid resolution (blue). The peaks in the plots indicate the corresponding forced wavenumbers k_f.

scales; the energy ($E_{\parallel}$) in the parallel (to $\mathbf{\Omega}$) component of velocity is much less than the average energy ($E_{\perp}$) in one of the perpendicular components. It is of importance to note that at smaller scales, the system is effectively isotropic since $A \sim 1$, and consequently the flow can be seen as a 3D turbulent flow where the effect of rotation is negligible.

B. Inverse energy cascade

The energy evolution equation may be written as

$$\frac{\partial E(k,t)}{\partial t} = T(k,t) - 2\nu k^2 E(k,t) + F(k,t), \tag{4}$$

where $T(k, t)$ is the energy transfer to the wavenumber shell k due to nonlinearity, $-2\nu k^2 E(k, t)$ is the energy dissipation spectrum, and $F(k, t)$ is the energy injected in the system by forcing. Away from the forcing scales, in steady state where $\frac{\partial E(k,t)}{\partial t} \approx 0$, Eq. (4) becomes

$$\frac{d\Pi(k)}{dk} \equiv -T(k) = -2\nu k^2 E(k). \tag{5}$$

$\Pi(k)$ is the kinetic energy flux, defined as the net transfer of energy out of the sphere of radius k by the modes inside the sphere. We can compute the energy flux of the system using the following formula:[62,63]

$$\Pi(k_*) = \sum_{k>k_*} \sum_{p\le k_*} S(\mathbf{k}|\mathbf{p}|\mathbf{q}), \tag{6}$$

where

$$S(\mathbf{k}|\mathbf{p}|\mathbf{q}) \equiv \mathrm{Im}[(\mathbf{k}\cdot\mathbf{u}(\mathbf{q}))(\mathbf{u}(\mathbf{p})\cdot\mathbf{u}^*(\mathbf{k}))] \tag{7}$$

is the mode-to-mode energy transfer rate from mode $\mathbf{p}$ to mode $\mathbf{k}$ with mode $\mathbf{q}$ as a mediator in the triad ($\mathbf{k}$, $\mathbf{p}$, $\mathbf{q}$; $\mathbf{k} = \mathbf{p} + \mathbf{q}$). The resulting figure, Fig. 2, explicitly depicts that at the scales larger than the scale at which forcing is active, there is an inverse cascade of energy that is reminiscent of a similar inverse cascade in the two-dimensional turbulence. As a result of this inverse cascade of the kinetic energy, there would be condensation of kinetic energy at lower wavenumbers. This is also seen in the decaying rotating turbulent system.[59] This condensation is naturally expected to give rise to the large scale coherent structures.

C. Large scale coherent structures

There is a large body of studies[23,30,59,64–69] on the formation of the large scale structures, which is known to depend on the strength of the rotation rate: at a very high rotation rate, the flow profile becomes quasi-two-dimensionalized with sharp coherent vortical columns, while at a low rotation

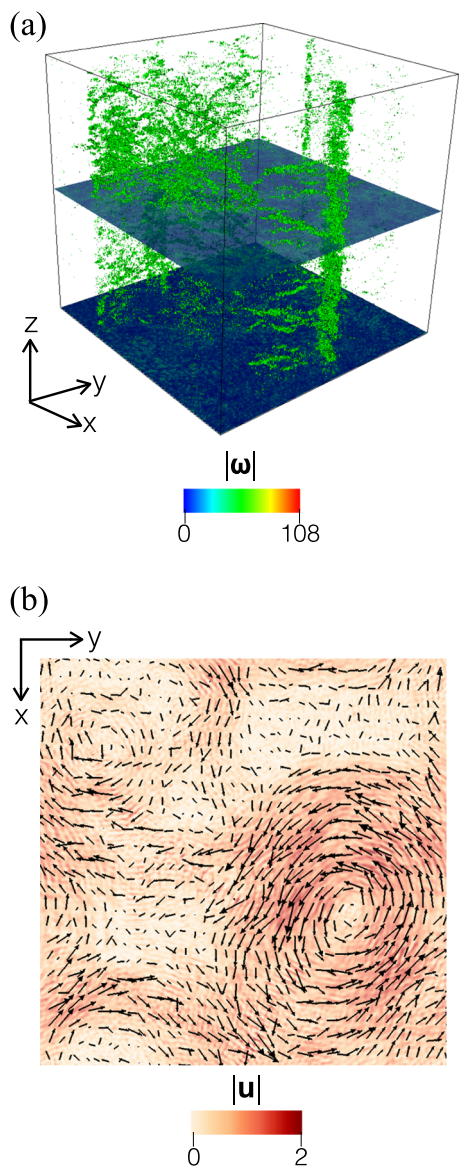

FIG. 3. Plots for (a) iso-surfaces of various magnitudes of the 3D vorticity field and (b) the density plot for the cross section of 2D velocity field taken at $z = \pi$. Both the plots use the 1024^3-grid simulation data.

rate, the columnar vortices are understandably disorganized. Figure 3(a) exhibits isosurfaces of constant $|\boldsymbol{\omega}|$ at $t = t_f$, where $\boldsymbol{\omega} = \nabla \times \mathbf{u}$ is the vorticity field. In Fig. 3(b), we plot the 2D velocity ($\mathbf{u} = u_x\hat{\mathbf{x}} + u_y\hat{\mathbf{y}}$) field for the horizontal cross section taken at $z = \pi$ of the flow profile. The figure shows vortical columns. We observe that the columnar vortices are disorganized and not very sharp in appearance. Compared to the decaying case,[59] in 3D forced rotating turbulence flow, the velocity in the direction of rotation is no longer constant, and the stretching and tilting of vortices occur. Also, in the plane perpendicular to the direction of rotation, the incompressible condition ($\nabla\cdot\mathbf{u}_\perp \neq 0$) is not satisfied and the two-dimensionalization is relatively hindered than what happens in the decaying case. Additionally, the forcing randomizes the flow, and it starts affecting the velocity field and obstructs the alignment of the vorticity field along the direction of rotation. This obstruction in alignment of velocity fields affects the structure formation in the forced rotating turbulent system.

In order to quantitatively understand the disorganization of the columnar structures in forced rotating turbulence, we study the energy content of the Fourier modes. Table II tabulates the energy contents of the most energetic Fourier modes for the forced rotating case at time frame $t = 56$ for the grid resolution of 512^3 and at $t = 3$ for 1024^3 grid resolution. We do not list the energy of $-\mathbf{k}$ modes because $\mathbf{u}(-\mathbf{k}) = \mathbf{u}^*(\mathbf{k})$. The fraction of the total energy contained in $18 \times 2 = 36$ Fourier modes is a significant amount of the total energy spread over 512^3 and 1024^3 modes. The Fourier modes $(k_x, k_y, k_z) = (1, 0, 0)$ and $(0, 1, 0)$ are the most dominant modes of the system. These modes contain 25–30 percent of the total energy of the system. The situation is different in the case of decaying rotating turbulence, where modes $(\pm1, 0, 0)$ and $(0, \pm1, 0)$ contain around 90 percent of the total energy.[59] It may be remarked that in the case of decaying turbulence these modes are not strong initially but later in time they become dominant. In comparison, however, there is no significant temporal variation in the kinetic energy distribution for the forced rotating turbulence, as can be gathered from Table II. The important thing to note is that, in the case of the forced rotating turbulent system, more energy is uniformly distributed in the other modes as should be expected for the relatively less coherent columns.

TABLE II. Percentage energy distribution among dominant modes at $t = 56$ and $t = 3$ for the grid resolution of 512^3 and 1024^3 at the rotation rate $\Omega = 32$, respectively. In the table, E_{mode} is defined as $E_{\text{mode}} = |u(\mathbf{k})|^2/2$ and E is the total energy of the system at $t = 3, 56$.

Mode (k_x, k_y, k_z)	E_{mode}/E (%) $t = 56$ $N = 512^3$	E_{mode}/E (%) $t = 3.0$ $N = 1024^3$
(1, 0, 0)	14.17	15.02
(0, 1, 0)	11.31	13.97
(1, 1, 0)	1.62	2.82
(−1, 1, 0)	1.43	0.45
(1, 2, 0)	0.92	1.77
(2, −1, 0)	0.51	0.40
(−2, 1, 0)	0.51	0.40
(2, 2, 0)	0.34	0.04
(1, −2, 0)	0.31	0.19
(−3, 1, 0)	0.31	0.22
(2, −2, 0)	0.21	0.12
(3, 1, 0)	0.13	0.06
(3, −2, 0)	0.13	0.06
(2, 1, 0)	0.13	0.23
(−1, −3, 0)	0.07	0.15
(−3, −2, 0)	0.05	0.44
(−2, −3, 0)	0.02	0.13
(−3, 0, 0)	0.02	0.06
Total %	32.19	36.53

IV. THE ENERGY SPECTRUM

The energy spectrum across the full range of wavenumbers is shown in Figs. 4(a) and 5. We note that about the forced scales (corresponding to the peaks in the plots), the spectrum is too disrupted to show any prominent scaling. We, thus, focus our attention on two different non-overlapping ranges of scales: the scales smaller than the forcing scales and the scales larger than the forcing scales.

It is obvious that the larger scales, being more affected by the rotation, should behave as if they are quasi-two-dimensionalized. By contrast, the smaller scales should have energy spectrum with an exponential term reminding one of the far dissipation ranges of the 3D isotropic homogeneous turbulence and the exponential fit found for the rapidly

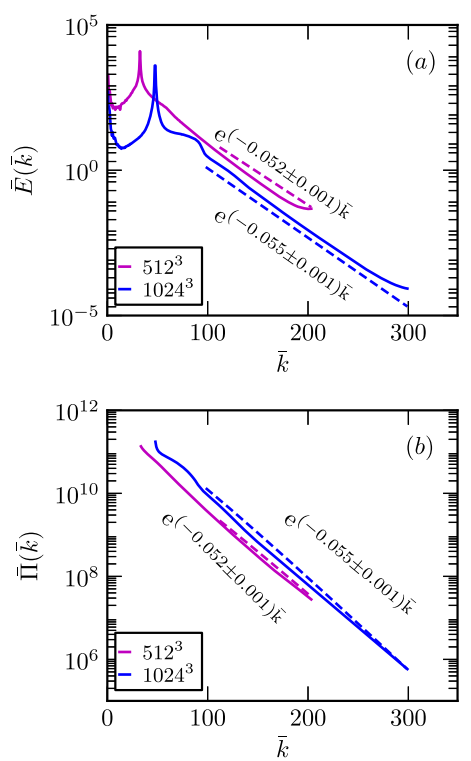

FIG. 4. Plots of (a) the non-dimensionalized energy spectra, $\bar{E}(\bar{k})$, and (b) the non-dimensionalized energy flux, $\bar{\Pi}(\bar{k})$, at $t = t_f$, as generated by the simulations performed with grid resolutions of 512^3 (magenta) and 1024^3 (blue) for the forced rotating turbulent fluid. The dotted lines are the fits generated in accordance with the energy spectra and the energy flux given in Eqs. (11) and (12).

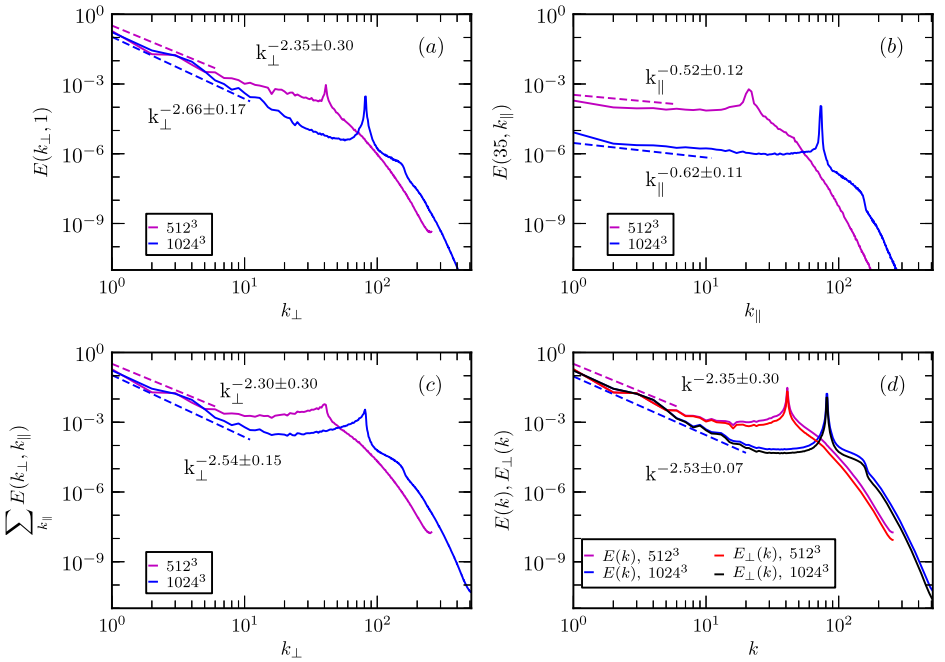

FIG. 5. Plots of the (anisotropic) energy spectrum $E(k_\perp, k_\parallel)$ at $t = t_f$, as a function of (a) $k_\perp$ for $k_\parallel = 1$, (b) $k_\parallel$ for $k_\perp = 35$, and (c) $k_\perp$ after the spectrum is summed over all $k_\parallel$. The dashed lines are the fitting lines; we have appropriately used the wavenumber range $1 \le k_\perp, k_\parallel \le 6$ for the 512^3 grid resolution and $1 \le k_\perp, k_\parallel \le 11$ for the 1024^3 grid resolution as the fitting ranges. As in the other plots, we have used magenta for 512^3 grid-resolution data and blue for 1024^3 grid-resolution data. Subplot (d) exhibits the plots for the (isotropic) energy spectra, $E(k)$ (magenta and blue) and $E(k_\perp)$ (red and black), as functions of k. Here, we have used additional colours—red and black—to, respectively, indicate the data corresponding to 512^3 grid resolution and 1024^3 grid resolution. The fitting ranges in subplot (d) are $1 \le k \le 6$ for 512^3 grid resolution and $1 \le k \le 20$ for 1024^3 grid resolution.

rotating decaying turbulence.[59] However, the energy spectra that we report in this paper for both the ranges ($k < k_f$ and $k > k_f$) are—to the best of our knowledge—unreported in any direct numerical simulations performed so far. In particular, we find that while the exponential fit in the decaying case goes as $\exp(-\text{constant} \times k^2)$, in the forced case, it goes as $\exp(-\text{constant} \times k^1)$ which is less steep in the dissipation range ($k > k_\eta, k_f$). Furthermore, in the anisotropic regime, i.e., in the larger scales ($k < k_f$), the Kuznetsov–Zakharov–Kolmogorov (KZK) spectrum[25] emerges. In what follows, we model and discuss these spectra in detail as discovered in our numerical simulations.

A. Model spectrum for smaller scales

Most models of the forced rotating turbulence predict Kolmogorov's $k^{-5/3}$ spectrum in the wavenumber range $k_\Omega, k_f < k < k_{\rm DI}$, where $k_{\rm DI}$ is the transition wavenumber (usually much smaller than k_η) between the inertial range and the dissipation range. Thus, in order to see this scaling, at the lower end, we need to pick the larger one between k_Ω and k_f. Unfortunately, in all our simulations, $k_\Omega > k_\eta$ and k_f is very close to k_η which is approximately just two to three times more than k_f. Because of this, there is no significant range of wavenumbers that could exhibit the $k^{-5/3}$ spectrum discernible in a log-log plot.

Recently, Verma *et al.*[70] and Verma[7] had shown that for laminar hydrodynamic flows, the steady state energy spectrum and the flux are proportional to $\exp(-k/k_\eta)/k$ and $\exp(-k/k_\eta)$, respectively. These functions satisfy Eq. (5) and also match with numerical simulations of the laminar flows. For our rapidly rotating flow, the energy content in the scales smaller than the forcing scale, $\sum_{k>k_f} E(k)$, is quite small; hence, it can be treated as approximately laminar. This is due to the strong inverse cascade of energy to the larger scales that retain most of the energy. Motivated by this observation, we propose the following form for $E(k)$ in the smaller scales extending into the far dissipation range:

$$E(k) \equiv \sum_{k-1<k'\le k} \frac{1}{2}|\hat{\mathbf{u}}(\mathbf{k}')|^2 = u_{\rm rms}^2 f_L(k) \frac{1}{k} \exp(-\alpha k/k_d). \quad (8)$$

From the form of this $E(k)$, it may be noted that Eq. (5) contains the effects of weak nonlinearity of the flow. The weak energy flux $\Pi(k)$ is the result of this nonlinearity.

The above $E(k)$ has only one exponent, viz., α, which needs to be determined. Here $u_{\rm rms}$ is the rms velocity of the high-pass filtered flow with all the component wave vectors greater than k_η. Note that we have introduced a new wavenumber k_d which is taken to be $\sqrt{\rm Re}/L$, but now Re is calculated with U replaced by $u_{\rm rms}$. In this context, recall that $k_\eta \equiv \left(\epsilon/\nu^3\right)^{1/4} \sim \sqrt{\rm Re}/L$, where

$$\epsilon = \int_0^\infty 2\nu k^2 E(k) dk = 2\nu u_{\rm rms}^2 k_d^2 I, \quad (9)$$

with $I \equiv \int_0^\infty \bar{k} f_L(\bar{k}) \exp(-\alpha\bar{k}) d\bar{k}$ and $\bar{k} \equiv k/k_d$. Thus, k_d based on the high-pass filtered flow is analogous to k_η which is based on the unfiltered flow field.

Using $\bar{k}$, $\bar{E}(\bar{k}) \equiv E(k)k/u_{\rm rms}^2$, and $\bar{\Pi}(\bar{k}) \equiv \Pi(k)/\epsilon$ as non-dimensionalized quantities, the relationship [Eq. (5)] between the kinetic energy and the energy flux in the non-dimensionalized form becomes

$$\frac{d\bar{\Pi}(\bar{k})}{d\bar{k}} = -\frac{\bar{k}}{I}\bar{E}(\bar{k}). \quad (10)$$

In the dissipation range $k \gg k_f$, where k_f is the forcing wavenumber and $f_L(\bar{k})$ is unity, the kinetic energy and the energy flux are, respectively, as follows:

$$\bar{E}(\bar{k}) = \exp(-\alpha\bar{k}), \quad (11)$$

$$\bar{\Pi}(\bar{k}) = \frac{1}{I}\left(\frac{1}{\alpha^2} + \frac{\bar{k}}{\alpha}\right)\exp(-\alpha\bar{k}). \quad (12)$$

It may be easily checked that the above two expressions satisfy the non-dimensionalized equation, Eq. (10).

In Figs. 4(a) and 4(b), we plot $\bar{E}(\bar{k})$ vs. $\bar{k}$ and $\bar{\Pi}(\bar{k})$ vs. $\bar{k}$, respectively, in semi-log scale at time frames $t = 56$ (magenta) for a grid resolution of 512^3 and at $t = 3$ (blue) for a grid resolution of 1024^3. We observe that the predicted self-consistent model [Eqs. (11) and (12)] of the energy spectrum and the energy flux stands validated by our numerical data in the wavenumber range $k \in [141, 256]$ for 512^3 grid resolution and $k \in [168, 512]$ for 1024^3 grid resolution. The values of α are 0.052 ± 0.001 for 512^3 grid resolution and 0.055 ± 0.001 for 1024^3 grid resolution. We are getting approximately the same value of α for both the grid resolutions, thus, signifying that the parameter is robust and resolution-independent. The values of Re based on the aforementioned wavenumber ranges are 62 for 512^3 and 115 for 1024^3 resolutions, which are one order less than the global Re (1736 and 1786, respectively, for the grid resolutions 512^3 and 1024^3). Thus, there is a reduction in the strength of turbulence in the smaller scales, which is the reason why any power law scaling is hard to observe here.

B. Model spectrum near larger scales

Although one can extract scaling exponents from the $E(k)$ vs. k plot to characterise the system; strictly speaking, in the anisotropic regime, the energy spectrum should not be modelled as a function of k. It is more sensible that the energy spectrum be explicitly dependent on both $\mathbf{k}_\perp$ (two dimensional vector perpendicular to the rotation axis) and $k_\parallel$ (wavenumber corresponding to the direction parallel to the rotation axis). Thus, we define such a spectrum as

$$E(k_\perp, k_\parallel) = \sum_{\substack{k_\perp - 1 < k'_\perp \le k_\perp, \\ k_\parallel - 1 < k'_\parallel \le k_\parallel}} \frac{1}{2} |\hat{\mathbf{u}}(k'_\perp, k'_\parallel)|^2. \tag{13}$$

Note that, under the assumption of axisymmetry, we have used the magnitude of $\mathbf{k}_\perp$ in the argument of the energy spectrum.

The energy spectrum of the system is calculated by using Eq. (13) and plotted in Fig. 5. In Figs. 5(a) and 5(b), it is remarkable to note that the energy spectrum observed from our numerical simulation is quite close to the Kuznetsov–Zakharov–Kolmogorov (KZK) spectrum—$E(k) \sim k_\perp^{-5/2} k_\parallel^{-1/2}$—within error bars. The strong rotation supplies a small parameter, Ro, in the framework of weak turbulence. Using this, it has shown[25] that, in the anisotropic limit $k_\perp \gg k_\parallel$, structures elongated along the rotation axis are brought forth through dominating local interactions. Furthermore, the KZK spectrum comes out as an exact solution. Although the aforementioned weak turbulence analysis has been performed for decaying rotating turbulent fluid, we emphasize that this spectrum appears in our numerical simulations exactly where the system is strongly anisotropic and shows elongated structures, thereby somewhat satisfying the requirements for the appearance of the spectrum. It may be noted, in this context, that the aforementioned plots are for the case $k_\perp \gg k_\parallel$, just what the weak turbulence analysis requires. We also note that the shift of the peaks away from k_f in Fig. 5(b) is because the abscissa is $k_\parallel$ and not k, and thus, the identity $k^2 = k_\perp^2 + k_\parallel^2$ with $k = k_f$ and $k_\perp = 35$ locates the peaks at $k_\parallel \approx 21$ and $k_\parallel \approx 74$, respectively, for 512^3 and 1024^3 grid resolutions.

Additionally, in Fig. 5(c), we note that the scaling exponent of $k_\perp$ is unchanged even when the spectrum is summed over all $k_\parallel$. Furthermore, Fig. 5(d) showcases the fact that this scaling exponent ($\sim -5/2$) is very robust; in the range $A \gg 1$, even the isotropic energy spectrum, $E(k)$, scales as $\sim k^{-5/2}$ and so does $E_\perp(k)$ simply because the share of energy contained in the plane perpendicular to the rotation axis is large. We remark that, however, the scaling exponent of $k_\parallel$ is not very robust and it varies with the choice of $k_\perp$ range (see Appendix B). Nevertheless, we believe that ours is the first numerical demonstration of KZK spectra in forced rotating turbulence.

V. DISCUSSIONS AND CONCLUSION

We have performed direct numerical simulations of a 3D turbulent fluid forced at intermediate scales. The fluid is rotating with a high rotation rate corresponding to Ro $\sim 10^{-3}$. Such a system is known to mimic some of the features of the 2D turbulence. Recall that in the fully developed 2D fluid turbulence—extensively investigated[10,11,71–79] numerically as well as experimentally—strong vortical structures appear in the system due to the inverse cascade of kinetic energy from the forcing scale to the scale corresponding to the box-size. Furthermore, it has been shown that the kinetic energy spectrum for $k < k_f$ is given by $E(k) \sim k^{-5/3}$, whereas[80–83] for $k > k_f$, $E(k) \sim k^{-3}$.

In the forced rotating flow, we observed that the system becomes highly anisotropic at larger scales; coherent columnar structures are formed, but they are relatively more diffused in appearance compared to what is seen in the case of decaying rotating turbulence. We have also found dual cascade regions—forward and reverse cascades—for both the energy and the enstrophy (calculated on a 2D horizontal plane; see Appendix A). While these features are very much reminiscent of the 2D turbulence, the forms of the energy spectrum on either side of k_f are completely different from what is observed in the 2D turbulence. Thus, the quasi-two-dimensionalization in the rotating 3D turbulent fluid does not actually mean that the spectral properties of the fluid become akin to that possessed by the 2D turbulent fluid.

For the anisotropic regime, we have also investigated the behavior of the kinetic energy spectrum as a function of $k_\perp$ and $k_\parallel$, which is convenient to showcase the manifestations of the anisotropic behavior of the system. We observed that the kinetic energy spectrum varies as $k_\perp^{-2.35\pm0.30}$ in the wavenumber range $k_\perp \in [1, 6]$ for a grid resolution of 512^3 and scales as $k_\perp^{-2.66\pm0.30}$ in the wavenumber range $k_\perp \in [1, 11]$ for a grid resolution of 1024^3. The kinetic energy spectrum as a function of $k_\parallel$ shows power scalings for fixed $k_\perp$, specifically, $E(35, k_\parallel) \sim k_\parallel^{-0.52\pm0.12}$ in the wavenumber range $k_\parallel \in [1, 6]$ for a grid resolution of 512^3 and $E(35, k_\parallel) \sim k_\parallel^{-0.62\pm0.11}$ in the wavenumber range $k_\parallel \in [1, 11]$ for 1024^3 grid resolution. Within the error bars, these scalings are in conformity with the KZK-spectrum. As far as the isotropic small scales are concerned, we have proposed a model [Eq. (8)] that faithfully captures the behavior of the kinetic energy spectrum in the far dissipation range. Our proposed model is in very good agreement with the numerical results over the wavenumber range $k \in [k_\eta, k_{\max}]$.

Our investigation highlights that the statistical features of the decaying rotating turbulence and the forced rotating turbulence are quite different. This fact suggests that a similar scientific comparison of the decaying versus the forced turbulences under the simultaneous effects of the rotation and the non-zero kinetic helicity is worth pursuing in the future. This is important because, in any realistic experiment of the forced rotating turbulence, the experimental setups are such that some finite amount of the kinetic helicity would invariably be imparted to the fluid. Also, the kinetic helicity is significant inside the Earth's outer core and is similarly important in the other planets and the stars.

ACKNOWLEDGMENTS

The authors thank Abhishek Kumar for many important suggestions. M.K.V. thanks the Department of Science and Technology, India (No. INT/RUS/RSF/P-03), and Russian Science Foundation, Russia (No. RSF-16-41-02012), for the Indo-Russian project. S.C. gratefully acknowledges financial support from the INSPIRE Faculty Fellowship (No. DST/INSPIRE/04/2013/000365) awarded by the INSA, India, and DST, India. The simulations were performed on the HPC2010 and HPC2013 and Chaos cluster of IIT Kanpur, India.

APPENDIX A: INVERSE ENSTROPHY CASCADE

We studied the enstrophy flux of the plane perpendicular to the axis of rotation. We compute the enstrophy flux of the $2D$ velocity field $\mathbf{u}_\perp$ at the plane using the formula

$$\Pi_\omega^{(2D)}(k_*) = \sum_{k>k_*}\sum_{p\le k_*} S^{\omega\omega}(\mathbf{k}|\mathbf{p}|\mathbf{q}). \tag{A1}$$

Here,

$$S^{\omega\omega}(\mathbf{k}|\mathbf{p}|\mathbf{q}) = \mathrm{Im}\Big[(\mathbf{k}\cdot\mathbf{u}_\perp(\mathbf{q}))\big(\omega_z(\mathbf{p})\omega_z^*(\mathbf{k})\big)\Big], \tag{A2}$$

with

$$\omega_z(\mathbf{k}) = [i\mathbf{k}\times\mathbf{u}(\mathbf{k})]_z \tag{A3}$$

represents the enstrophy transfer from mode $\omega_z(\mathbf{p})$ to mode $\omega_z(\mathbf{k})$ with mode $\mathbf{u}(\mathbf{q})$ acting as a mediator. Figure 6 illustrates the enstrophy flux of the horizontal cross section taken at $z = \pi$ at time frame $t = 56$ (magenta) for a grid resolution of 512^3 and at $t = 3$ (blue) for 1024^3 grid resolution. Arguably,[83] when the vortex merger is strong in 2D turbulent flow, the mean enstrophy flux is negative[84,85] for the scales larger than the injection scales. Therefore, the negative enstrophy flux in the scales larger than the injection scale (as exhibited in Fig. 6) signifies that our rotating 3D flow is appreciably two-dimensionalized.

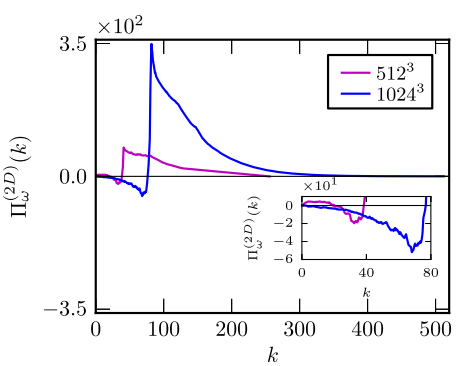

FIG. 6. Plot of the 2D enstrophy flux, $\Pi_\omega^{(2D)}(k)$, for the 2D velocity field on the horizontal cross section, $z = \pi$, at $t = t_f$ for the grid-resolutions 512^3 (magenta) and 1024^3 (blue). The inset highlights the inverse cascade of the flux. The peaks in the plots indicate the corresponding forced wavenumbers k_f.

APPENDIX B: ANISOTROPIC ENERGY SPECTRUM'S SCALING WITH $k_\parallel$

The KZK spectrum exists in the anisotropic limit, viz., $k_\perp \gg k_\parallel$, in rapidly rotating turbulence as was shown by Galtier[25] (and we have observed so in Fig. 5); however, that analysis did not include forcing. Since our investigation is for the forced rotating turbulent fluid, we must keep this added complication in mind while extracting the exponent of $k_\parallel$ in the anisotropic energy spectrum. The scaling of the energy spectrum as a function of $k_\parallel$ depends on the choice of $k_\perp$ in the anisotropic limit, which is shown in Fig. 7.

In Fig. 7, we plot the energy spectrum as a function of $k_\parallel$ for different $k_\perp$ for both the 512^3 grid resolution and the 1024^3 grid resolution. In order to extract the exponent, we have to decide not only what range of $k_\parallel$ to use but also what value of $k_\perp$ to choose. Although one would like to choose a large enough range while maintaining $k_\perp \gg k_\parallel$, we are restricted in our choice because the peak corresponding to the forcing scale restricts us: the upper bound of the fitting range should

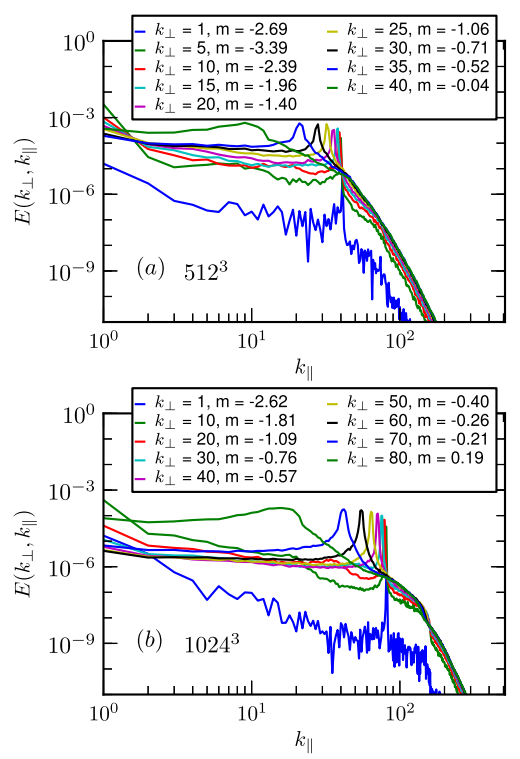

FIG. 7. Plots of the (anisotropic) energy spectrum, $E(k_\perp, k_\parallel)$ at $t = t_f$, as a function of $k_\parallel$ with different $k_\perp$ for (a) 512^3 grid resolution and (b) 1024^3 grid resolution. The fitting exponent (m) in $E(k_\perp, k_\parallel) \sim k_\parallel^{-m}$ has been calculated in the wavenumber range $1 \le k_\parallel \le 6$ for the 512^3 grid resolution and $1 \le k_\parallel \le 11$ for the 1024^3 grid resolution and is shown in the legends.

ideally be as much away from the forcing scale as possible, but the peak shift toward a lower wavenumber, in line with the identity $k^2 = k_\perp^2 + k_\parallel^2$, as $k_\perp$ increases, thereby making the range smaller. This is at odds with the fact that $k_\perp$ must be much greater than $k_\parallel$ for witnessing the KZK spectrum. Thus, it effectively becomes a matter of systematic investigation where one should work with all possible combinations of the $k_\parallel$-ranges and the value of $k_\perp$. What we can definitely conclude from Fig. 7 is that for 512^3 grid resolution, the range $1 \le k_\parallel \le 6$ and $k_\perp = 35$ make an ideal combination which leads to the observation of the KZK-spectrum in the anisotropic limit in the forced rotating turbulence. Similar conclusion can be made for the 1024^3 grid resolution with the range $1 \le k_\parallel \le 11$ and $k_\perp = 35$.

[1] P. A. Davidson, *Turbulence in Rotating, Stratified and Electrically Conducting Fluids* (Cambridge University Press, Cambridge, UK, 2013).
[2] A. N. Kolmogorov, "The local structure of turbulence in incompressible viscous fluid for very large Reynolds numbers," Dokl. Akad. Nauk SSSR **30**, 301–305 (1941).
[3] A. N. Kolmogorov, "Dissipation of energy in locally isotropic turbulence," Dokl. Akad. Nauk SSSR **32**, 16–18 (1941).
[4] G. E. Elsinga and I. Marusic, "The anisotropic structure of turbulence and its energy spectrum," Phys. Fluids **28**, 011701 (2016).
[5] P. C. Valente, C. B. da Silva, and F. T. Pinho, "Energy spectra in elasto-inertial turbulence," Phys. Fluids **28**, 075108 (2016).
[6] S. S. Pawar and J. H. Arakeri, "Kinetic energy and scalar spectra in high Rayleigh number axially homogeneous buoyancy driven turbulence," Phys. Fluids **28**, 065103 (2016).
[7] M. K. Verma, *Physics of Buoyant Flows: From Instabilities to Turbulence* (World Scientific, Singapore, 2018).
[8] P. Buchhave and C. M. Velte, "Measurement of turbulent spatial structure and kinetic energy spectrum by exact temporal-to-spatial mapping," Phys. Fluids **29**, 085109 (2017).
[9] R. H. Kraichnan, "Inertial ranges in two-dimensional turbulence," Phys. Fluids **10**, 1417 (1967).
[10] J. Paret and P. Tabeling, "Experimental observation of the two-dimensional inverse energy cascade," Phys. Rev. Lett. **79**, 4162 (1997).
[11] S. Chen, R. E. Ecke, G. L. Eyink, M. Rivera, M. Wan, and Z. Xiao, "Physical mechanism of the two-dimensional inverse energy cascade," Phys. Rev. Lett. **96**, 084502 (2006).
[12] A. Vallgren and E. Lindborg, "The enstrophy cascade in forced two-dimensional turbulence," J. Fluid Mech. **671**, 168–183 (2011).
[13] G. Boffetta and R. E. Ecke, "Two-dimensional turbulence," Annu. Rev. Fluid. Mech. **44**, 427–451 (2012).
[14] A. Ibbetson and D. J. Tritton, "Experiments on turbulence in a rotating fluid," J. Fluid Mech. **68**, 639–672 (1975).
[15] E. J. Hopfinger, F. K. Browand, and Y. Gagne, "Turbulence and waves in a rotating tank," J. Fluid Mech. **125**, 505–534 (1982).
[16] J. Bardina, J. H. Ferziger, and R. S. Rogallo, "Effect of rotation on isotropic turbulence: Computation and modelling," J. Fluid Mech. **154**, 321–336 (1985).
[17] L. Jacquin, O. Leuchter, C. Cambon, and J. Mathieu, "Homogeneous turbulence in the presence of rotation," J. Fluid Mech. **220**, 1–52 (1990).
[18] O. Zeman, "A note on the spectra and decay of rotating homogeneous turbulence," Phys. Fluids **6**, 3221–3224 (1994).
[19] Y. Zhou, "A phenomenological treatment of rotating turbulence," Phys. Fluids **7**, 2092 (1995).
[20] V. M. Canuto and M. S. Dubovikov, "Physical regimes and dimensional structure of rotating turbulence," Phys. Rev. Lett. **78**, 666–669 (1997).
[21] V. M. Canuto and M. S. Dubovikov, "A dynamical model for turbulence. V. The effect of rotation," Phys. Fluids **9**, 2132–2140 (1997).
[22] P. K. Yeung and Y. Zhou, "Numerical study of rotating turbulence with external forcing," Phys. Fluids **10**, 2895–2909 (1998).
[23] L. M. Smith and F. Waleffe, "Transfer of energy to two-dimensional large scales in forced, rotating three-dimensional turbulence," Phys. Fluids **11**, 1608 (1999).
[24] C. N. Baroud, B. B. Plapp, Z.-S. She, and H. L. Swinney, "Anomalous self-similarity in a turbulent rapidly rotating fluid," Phys. Rev. Lett. **88**, 114501 (2002).
[25] S. Galtier, "Weak inertial-wave turbulence theory," Phys. Rev. E **68**, 015301 (2003).
[26] Y. Hattori, R. Rubinstein, and A. Ishizawa, "Shell model for rotating turbulence," Phys. Rev. E **70**, 046311 (2004).
[27] X. Yang and J. A. Domaradzki, "Large eddy simulations of decaying rotating turbulence," Phys. Fluids **16**, 4088–4104 (2004).
[28] J. E. Ruppert-Felsot, O. Praud, E. Sharon, and H. L. Swinney, "Extraction of coherent structures in a rotating turbulent flow experiment," Phys. Rev. E **72**, 016311 (2005).
[29] L. M. Smith and Y. Lee, "On near resonances and symmetry breaking in forced rotating flows at moderate Rossby number," J. Fluid Mech. **535**, 111–142 (2005).
[30] C. Morize, F. Moisy, and M. Rabaud, "Decaying grid-generated turbulence in a rotating tank," Phys. Fluids **17**, 095105 (2005).
[31] W.-C. Müller and M. Thiele, "Scaling and energy transfer in rotating turbulence," Europhys. Lett. **77**, 34003 (2007).
[32] S. Chakraborty and J. K. Bhattacharjee, "Third-order structure function for rotating three-dimensional homogeneous turbulent flow," Phys. Rev. E **76**, 036304 (2007).
[33] S. Chakraborty, "Signatures of two-dimensionalisation of 3D turbulence in the presence of rotation," Europhys. Lett. **79**, 14002 (2007).
[34] M. Thiele and W.-C. Müller, "Structure and decay of rotating homogeneous turbulence," J. Fluid Mech. **637**, 425–442 (2009).
[35] P. D. Mininni, A. Alexakis, and A. Pouquet, "Scale interactions and scaling laws in rotating flows at moderate Rossby numbers and large Reynolds numbers," Phys. Fluids **21**, 015108 (2009).
[36] S. Chakraborty, M. H. Jensen, and A. Sarkar, "On two-dimensionalization of three-dimensional turbulence in shell models," Eur. Phys. J. B **73**, 447–453 (2010).
[37] A. Sen, P. D. Mininni, D. Rosenberg, and A. Pouquet, "Anisotropy and nonuniversality in scaling laws of the large-scale energy spectrum in rotating turbulence," Phys. Rev. E **86**, 036319 (2012).
[38] L. Biferale, F. Bonaccorso, I. M. Mazzitelli, M. A. T. van Hinsberg, A. S. Lanotte, S. Musacchio, P. Perlekar, and F. Toschi, "Coherent structures and extreme events in rotating multiphase turbulent flows," Phys. Rev. X **6**, 041036 (2016).
[39] Y. B. Baqui, P. A. Davidson, and A. Ranjan, "Are there two regimes in strongly rotating turbulence?," Phys. Fluids **28**, 045103 (2016).
[40] M. Hossain, "Reduction in the dimensionality of turbulence due to a strong rotation," Phys. Fluids **6**, 1077–1080 (1994).
[41] L. M. Smith, J. R. Chasnov, and F. Waleffe, "Crossover from two- to three-dimensional turbulence," Phys. Rev. Lett. **77**, 2467–2470 (1996).
[42] A. Pouquet, A. Sen, D. Rosenberg, P. D. Mininni, and J. Baerenzung, "Inverse cascades in turbulence and the case of rotating flows," Phys. Scr. **T155**, 014032 (2013).
[43] E. Yarom, Y. Vardi, and E. Sharon, "Experimental quantification of inverse energy cascade in deep rotating turbulence," Phys. Fluids **25**, 085105 (2013).
[44] A. Campagne, B. Gallet, F. Moisy, and P.-P. Cortet, "Direct and inverse energy cascades in a forced rotating turbulence experiment," Phys. Fluids **26**, 125112 (2014).
[45] L. Bourouiba, D. N. Straub, and M. L. Waite, "Non-local energy transfers in rotating turbulence at intermediate Rossby number," J. Fluid Mech. **690**, 129–147 (2012).
[46] R. H. Kraichnan, "The structure of isotropic turbulence at very high Reynolds numbers," J. Fluid Mech. **5**, 497–543 (1959).
[47] Y.-H. Pao, "Structure of turbulent velocity and scalar fields at large wavenumbers," Phys. Fluids **8**, 1063 (1965).
[48] S. B. Pope, *Turbulent Flows* (Cambridge University Press, Cambridge, 2000).
[49] L. M. Smith and W. C. Reynolds, "The dissipation-range spectrum and the velocity-derivative skewness in turbulent flows," Phys. Fluids A **3**, 992 (1991).
[50] K. R. Sreenivasan, "On the fine-scale intermittency of turbulence," J. Fluid Mech. **151**, 81–103 (1985).
[51] C. Foias, O. Manley, and L. Sirovich, "Empirical and Stokes eigenfunctions and far-dissipative turbulent spectrum," Phys. Fluids A **2**, 464 (1990).
[52] T. Sanada, "Comment on the dissipation-range spectrum in turbulent flows," Phys. Fluids A **4**, 1086 (1992).
[53] O. P. Manley, "The dissipation range spectrum," Phys. Fluids A **4**, 1320 (1992).
[54] D. O. Martínez, S. Chen, G. D. Doolen, R. H. Kraichnan, L.-P. Wang, and Y. Zhou, "Energy spectrum in the dissipation range of fluid turbulence," J. Plasma Phys. **57**, 195–201 (1997).

[55]S. Kida and Y. Murakami, "Kolmogorov similarity in freely decaying turbulence," Phys. Fluids **30**, 2030 (1987).
[56]J. A. Domaradzki, "Nonlocal triad interactions and the dissipation range of isotropic turbulence," Phys. Fluids A **4**, 2037 (1992).
[57]S. Chen, G. D. Doolen, J. R. Herring, R. H. Kraichnan, S. A. Orszag, and Z.-S. She, "Far-dissipation range of turbulence," Phys. Rev. Lett. **70**, 3051 (1993).
[58]S. G. Saddoughi and S. V. Veeravalli, "Local isotropy in turbulent boundary layers at high Reynolds number," J. Fluid Mech. **268**, 333–372 (1994).
[59]M. K. Sharma, A. Kumar, M. K. Verma, and S. Chakraborty, "Statistical features of rapidly rotating decaying turbulence: Enstrophy and energy spectra and coherent structures," Phys. Fluids **30**, 045103 (2018).
[60]M. K. Verma, A. G. Chatterjee, K. S. Reddy, R. K. Yadav, S. Paul, M. Chandra, and R. Samtaney, "Benchmarking and scaling studies of pseudospectral code Tarang for turbulence simulations," Pramana **81**, 617–629 (2013).
[61]A. G. Chatterjee, M. K. Verma, A. Kumar, R. Samtaney, B. Hadri, and R. Khurram, "Scaling of a fast Fourier transform and a pseudo-spectral fluid solver up to 196608 cores," J. Parallel Distrib. Comput. **113**, 77–91 (2018).
[62]G. Dar, M. K. Verma, and V. Eswaran, "Energy transfer in two-dimensional magnetohydrodynamic turbulence: Formalism and numerical results," Physica D **157**, 207–225 (2001).
[63]M. K. Verma, "Statistical theory of magnetohydrodynamic turbulence: Recent results," Phys. Rep. **401**, 229–380 (2004).
[64]P. Bartello, O. Metais, and M. Lesieur, "Coherent structures in rotating three-dimensional turbulence," J. Fluid Mech. **273**, 1–29 (1994).
[65]F. S. Godeferd and L. Lollini, "Direct numerical simulations of turbulence with confinement and rotation," J. Fluid Mech. **393**, 257–308 (1999).
[66]P. J. Staplehurst, P. A. Davidson, and S. B. Dalziel, "Structure formation in homogeneous freely decaying rotating turbulence," J. Fluid Mech. **598**, 81–105 (2008).
[67]F. Moisy, C. Morize, M. Rabaud, and J. Sommeria, "Decay laws, anisotropy and cyclone–anticyclone asymmetry in decaying rotating turbulence," J. Fluid Mech. **666**, 5–35 (2011).
[68]B. Gallet, A. Campagne, P. P. Cortet, and F. Moisy, "Scale-dependent cyclone-anticyclone asymmetry in a forced rotating turbulence experiment," Phys. Fluids **26**, 035108 (2014).
[69]A. Ranjan and P. A. Davidson, "Evolution of a turbulent cloud under rotation," J. Fluid Mech. **756**, 488–509 (2014).
[70]M. K. Verma, A. Kumar, P. Kumar, S. Barman, A. G. Chatterjee, R. Samtaney, and R. A. Stepanov, "Energy fluxes and spectra in the dissipation range of turbulent and laminar flows," Fluid Dyn. (to be published).
[71]V. Borue, "Spectral exponents of enstrophy cascade in stationary two-dimensional homogeneous turbulence," Phys. Rev. Lett. **71**, 3967 (1993).
[72]L. M. Smith and V. Yakhot, "Bose condensation and small-scale structure generation in a random force driven 2D turbulence," Phys. Rev. Lett. **71**, 352–355 (1993).
[73]G. Boffetta, A. Cenedese, S. Espa, and S. Musacchio, "Effects of friction on 2D turbulence: An experimental study of the direct cascade," Europhys. Lett. **71**, 590–596 (2005).
[74]M. A. Rutgers, "Forced 2D turbulence: Experimental evidence of simultaneous inverse energy and forward enstrophy cascades," Phys. Rev. Lett. **81**, 2244 (1998).
[75]T. Gotoh, "Energy spectrum in the inertial and dissipation ranges of two-dimensional steady turbulence," Phys. Rev. E **57**, 2984–2991 (1998).
[76]N. Schorghofer, "Energy spectra of steady two-dimensional turbulent flows," Phys. Rev. E **61**, 6572–6577 (2000).
[77]E. Lindborg and K. Alvelius, "The kinetic energy spectrum of the two-dimensional enstrophy turbulence cascade," Phys. Fluids **12**, 945–947 (2000).
[78]T. Ishihara and Y. Kaneda, "Energy spectrum in the enstrophy transfer range of two-dimensional forced turbulence," Phys. Fluids **13**, 544–547 (2001).
[79]Q. Chen, S. Chen, G. L. Eyink, and K. R. Sreenivasan, "Kolmogorov's third hypothesis and turbulent sign statistics," Phys. Rev. Lett. **90**, 254501 (2003).
[80]V. Borue, "Inverse energy cascade in stationary two-dimensional homogeneous turbulence," Phys. Rev. Lett. **72**, 1475–1478 (1994).
[81]C. V. Tran and J. C. Bowman, "Robustness of the inverse cascade in two-dimensional turbulence," Phys. Rev. E **69**, 036303 (2004).
[82]M. Chertkov, C. Connaughton, I. Kolokolov, and V. Lebedev, "Dynamics of energy condensation in two-dimensional turbulence," Phys. Rev. Lett. **99**, 084501 (2007).
[83]P. Fischer and C.-H. Bruneau, "Wavelet-based analysis of enstrophy transfers in two-dimensional turbulence," Phys. Fluids **21**, 065109 (2009).
[84]K. Ohkitani, "Wave number space dynamics of enstrophy cascade in a forced two-dimensional turbulence," Phys. Fluids A **3**, 1598 (1991).
[85]A. Babiano and A. Provenzale, "Coherent vortices and tracer cascades in two-dimensional turbulence," J. Fluid Mech. **574**, 429–448 (2007).